Electronic transport through a graphene-based ferromagnetic/normal/ferromagnetic junction

2010 J. Phys.: Condens. Matter 22 035301

(http://iopscience.iop.org/0953-8984/22/3/035301)

J. Phys.: Condens. Matter **22** (2010) 035301 (8pp) doi:10.1088/0953-8984/22/3/035301

Electronic transport through a graphene-based ferromagnetic/normal/ferromagnetic junction

Jiang-chai Chen[1], **Shu-guang Cheng**[2], **Shun-Qing Shen**[3] and **Qing-feng Sun**[1]

[1] Beijing National Lab for Condensed Matter Physics and Institute of Physics, Chinese Academy of Sciences, Beijing 100190, People's Republic of China
[2] Department of Physics, Northwest University, Xi'an 710069, People's Republic of China
[3] Department of Physics, and Center of Theoretical and Computational Physics, The University of Hong Kong, Hong Kong, People's Republic of China

E-mail: sunqf@aphy.iphy.ac.cn

Received 21 August 2009, in final form 10 November 2009
Published 21 December 2009
Online at stacks.iop.org/JPhysCM/22/035301

Abstract

Electronic transport in a graphene-based ferromagnetic/normal/ferromagnetic junction is investigated by means of the Landauer–Büttiker formalism and the nonequilibrium Green function technique. For the zigzag edge case, the results show that the conductance is always larger than e^2/h for the parallel configuration of lead magnetizations, but for the antiparallel configuration the conductance becomes zero because of the band-selective rule. Therefore, a magnetoresistance (MR) plateau emerges with the value 100% when the Fermi energy is located around the Dirac point. In addition, choosing narrower graphene ribbons can yield wider 100% MR plateaus and the length change of the central graphene region does not affect the 100% MR plateaus. Although the disorder will reduce the MR plateau, the plateau value can still be kept about 50% even in a large disorder strength case. In addition, when the magnetizations of the left and right leads have a relative angle, the conductance changes as a cosine function of the angle. What is more, for the armchair edge case, the MR is usually small. So, it is more favorable to fabricate a graphene-based spin valve device by using a zigzag edge graphene ribbon.

(Some figures in this article are in colour only in the electronic version)

1. Introduction

Graphene, a two-dimensional single-layer crystal of carbon atoms arrayed in a honeycomb lattice, is a novel and exciting material [1]. The low energy excitation of graphene has a linear dispersion relation, and the dynamics of the charge carriers obeys a massless Dirac-like equation [2]. Because of the unique band structures, graphene has many peculiar properties, such as Hall plateaus occurring at half-integer multiples of ge^2/h with the spin and valley degeneracy $g = 4$, and a conductivity at the zero magnetic field having a non-zero minimal value [3]. For neutral graphene, the Fermi level is located at the Dirac points, the corners of the hexagonal first Brillouin zone. In experiment, a gate voltage can be used to tune the Fermi level, which can then be above or below the Dirac points [4]. In addition, graphene also exhibits many excellent transport characteristics: a high mobility [5], long spin relaxation length [6], and stable behavior under ambient conditions. At room temperature, its mobility can be above 10^4 cm^2 V^{-1} s^{-1}, implying that the mean free path can be as long as a few hundred nanometers. Because of weak spin–orbit coupling [7] and a low hyperfine interaction [8], its spin

relaxation length can reach the order of a micron at room temperature. Thus, graphene may be an excellent candidate for microelectronic applications, in particular for spintronic applications [9].

In general, the charge carriers in graphene are not spin-polarized. For spintronic applications, people try to inject a spin-polarized current or induce spin-polarized carriers in graphene. Recently, many works have focused on this issue. For example, Haugen *et al* [10] suggested that spin-polarized carriers can be realized by growing graphene on a ferromagnetic (FM) insulator (e.g. EuO). Owing to the magnetic proximity effect, an exchange split between the spin-up and spin-down carriers in the graphene is induced, and then the carriers are spin-polarized. Based on the first-principles calculations, Son *et al* [11] predicted that the zigzag graphene nanoribbon becomes a half metal when an in-plane transverse electric field is applied. Also, Lin *et al* [12] demonstrated that electron–electron correlation in an armchair graphene nanoribbon can generate flat-band ferromagnetism. On the experimental side, a large spin injection into graphene has been realized by connecting it to an FM electrode [6, 13, 14]. Furthermore, several groups [14, 15] have performed nonlocal magnetoresistance (MR) measurements, in which a net spin current is brought between the injector and detector.

A well-known application in spintronics is the spin valve effect [16], in which the resistance of devices can be changed by manipulating the relative orientation of the magnetizations. Motivated by the spintronic application with the novel material, spin-polarized transport through graphene is currently attracting a great deal of attention [17–23]. Using the tight-binding model, Brey and Fertig [20] studied the MR of a FM/graphene/FM junction in the limit of infinite width. They found that the MR is rather small since the conductivity is weakly dependent on the relative magnetization orientations of the FM leads. Ding *et al* [21] investigated a similar device with two FM leads by a continuous model. The results showed that the MR versus the bias exhibits a cusp around zero bias in absence of an external magnetic field, and oscillating behavior at a high magnetic field. Based on the first-principles calculation, Kim and Kim [22] predicted that a graphene-based spin valve device could have a high MR.

In this paper, we study the conductance and MR of a graphene-based spin valve. The device consists of a graphene nanoribbon coupling to two FM leads, as shown in figure 1(a). Here the width of the device is finite in the order of 10 nm, i.e. the size effect is considered. In recent experiments [24], a few 10 nm or sub-10 nm graphene nanoribbons have already been fabricated successfully. For a finite-width graphene nanoribbon, the wavevectors along the confined direction are discrete, and transverse subbands emerge. The characteristics of the subbands are strongly dependent on the chirality of the graphene nanoribbon edge [25], e.g. the zigzag edge or armchair edge. So the conductance and MR should be strongly dependent on the boundary condition of the graphene nanoribbon. In addition, we consider that the two FM leads also have the same hexagonal lattice structure as the graphene. In other words, the leads are graphene-based FM or called FM graphene. In the experiment, the FM electrode (e.g. the cobalt electrode) usually overlaps the graphene through a thin oxide layer [6, 14]. Because of the magnetic proximity effect and the Zeeman effect, an exchange split in the graphene underneath the oxide layer is induced, and its carriers are spin-polarized. So the graphene covered with the FM electrode has magnetization. Thus, the spin-polarized charge carriers, driven by a bias, travel from one FM graphene through the central normal graphene to another FM graphene.

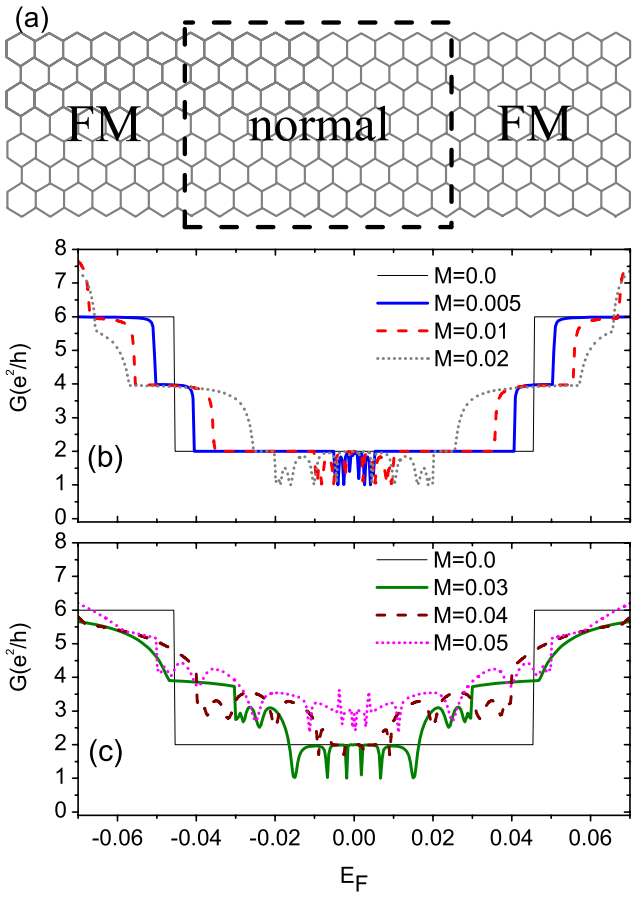

Figure 1. (a) The schematic of a graphene-based FM/normal/FM junction. (b), (c) The conductance G versus the Fermi energy E_F for different magnetizations M at the parallel configuration ($\theta = 0$). The size of the central graphene is $N = 50$ and $L = 10$.

In the tight-binding model the Landauer–Büttiker formula and the nonequilibrium Green function method are applied to calculate the conductance and MR. For the zigzag graphene ribbon case, we found that when the graphene nanoribbon is narrow enough, and its separation $\triangle$ between the first subband and the zeroth subband is larger than the exchange split energy M, the conductance for the antiparallel magnetization configuration can almost be zero in a quite large energy window around the Dirac point. However, for the parallel configuration the conductance is always larger than e^2/h, so the MR exhibits a plateau with the value 100%. As the width of the nanoribbon increases, the subband separation $\triangle$ gradually decreases, and the MR can maintain a value 100% at the beginning of $\triangle > M$, then decrease when $\triangle < M$. In the presence of disorder, the MR drops slightly, but even with quite a large disorder it can maintain the value 50%,

which is still much larger than 10%, the lower limit of the giant magnetoresistance effect. What is more, for the armchair graphene nanoribbon case, the MR is always small regardless of the width of nanoribbon. By comparing two cases of graphene ribbons with different edges, it is more reasonable to apply zigzag graphene ribbons to spin valve devices.

The rest of the paper is organized as follows: in section 2, we describe the model and details of the calculations. In sections 3 and 4 we will give the numerical results of the conductance and MR for the zigzag and armchair edge cases, respectively. Finally, a brief conclusion is presented in section 5.

2. Model and formulations

We consider a graphene-based spin valve (as shown in figure 1(a)) which consists of a central normal graphene strip and two FM graphene ribbons. The total Hamiltonian, H, of the device can be divided into four terms, $H = H_{\rm C} + H_{\rm L} + H_{\rm R} + H_{\rm T}$, where $H_{\rm C}$ describes the central normal graphene region, $H_{\rm L}$ and $H_{\rm R}$ are the Hamiltonians of the left and right FM graphene leads, respectively, and $H_{\rm T} = H_{\rm TL} + H_{\rm TR}$ is the coupling Hamiltonian of the central region to the left and right leads. In the tight-binding approximation [26], the Hamiltonians $H_{\rm C}$, $H_{\rm L}$, $H_{\rm R}$, and $H_{\rm T}$ can be written as

$$H_{\rm C} = \sum_{i\in C} \epsilon_{\rm C} a_i^\dagger \sigma_I a_i - \sum_{\langle ij\rangle (i,j\in C)} (t a_i^\dagger \sigma_I a_j + {\rm h.c.}),$$

$$H_{\alpha={\rm L,R}} = \sum_{i\in\alpha} a_i^\dagger (\epsilon_\alpha \sigma_I + \boldsymbol{\sigma}\cdot\mathbf{M}_\alpha) a_i - \sum_{\langle ij\rangle (i,j\in\alpha)} (t a_i^\dagger \sigma_I a_j + {\rm h.c.}),$$

$$H_{\rm T} = - \sum_{\langle ij\rangle (i\in C, j\in {\rm L,R})} (t a_i^\dagger \sigma_I a_j + {\rm h.c.}),$$

where $s = \uparrow, \downarrow$ represents the spin of electrons; $a_{is}^\dagger$ (a_{is}) creates (annihilates) an electron with spin s on-site i, and $a_i = \binom{a_{i\uparrow}}{a_{i\downarrow}}$; $\langle ij\rangle$ stands for a nearest-neighbor pair. $\boldsymbol{\sigma} = (\sigma_x, \sigma_y, \sigma_z)$ are the Pauli matrices and σ_I is a 2×2 unit matrix. $\epsilon_{\rm C}$, $\epsilon_{\rm L}$, and $\epsilon_{\rm R}$ are the on-site energies (i.e. the energy of the Dirac point) in the center region, left and right FM leads, respectively, which can be tuned by the gate voltage. The size of the center graphene region is described by the width N and length L. In figure 1(a), a zigzag edge graphene nanoribbon with $N = 4$ and $L = 9$ is shown. The terms, including the factor t in Hamiltonian, describe nearest-neighbor hopping with a hopping energy t. $\mathbf{M}_{\rm L}$ and $\mathbf{M}_{\rm R}$ are the magnetizations of the left and right FM leads. Here we allow the magnetizations $\mathbf{M}_{\rm L}$ and $\mathbf{M}_{\rm R}$ to be along arbitrary directions. Without loss of generality we assume that the magnetization $\mathbf{M}_{\rm L}$ of the left lead is along the z-axis, then $\mathbf{M}_{\rm L} = M_{\rm L}(0,0,1)$, and the magnetization $\mathbf{M}_{\rm R}$ of the right lead is along the direction (θ,φ) with $\mathbf{M}_{\rm R} = M_{\rm R}(\sin\theta\cos\varphi, \sin\theta\sin\varphi, \cos\theta)$.

Before performing the calculation, we take a unitary transformation with $\tilde{a}_i = U a_i$ for all sites i in the right FM lead, where the unitary matrix U is

$$U = \begin{pmatrix} \cos(\theta/2) & {\rm e}^{-{\rm i}\varphi}\sin(\theta/2) \\ {\rm e}^{{\rm i}\varphi}\sin(\theta/2) & -\cos(\theta/2) \end{pmatrix}.$$

Under this unitary transformation, the Hamiltonians $H_{\rm C}$, $H_{\rm L}$, and $H_{\rm TL}$ remain unchanged, and $H_{\rm R}$ and $H_{\rm TR}$ become

$$H_{\rm R} = \sum_{i\in R} \tilde{a}_i^\dagger (\epsilon_{\rm R}\sigma_I + \boldsymbol{\sigma}\cdot\mathbf{M}'_{\rm R})\tilde{a}_i - \sum_{\langle ij\rangle (i,j\in R)} (t\tilde{a}_i^\dagger \sigma_I \tilde{a}_j + {\rm h.c.}),$$

$$H_{\rm TR} = - \sum_{\langle ij\rangle (i\in C, j\in R)} (t a_i^\dagger U \tilde{a}_j + {\rm h.c.}),$$

where $\mathbf{M}'_{\rm R} = M_{\rm R}(0,0,1)$. After the unitary transformation, the z-axis of the spin in the right FM lead is along the direction of $\mathbf{M}'_{\rm R}$, and the Hamiltonian $H_{\rm R}$ is diagonal in the spin space.

The current flowing through the device can be calculated from the Landauer–Büttiker formula [27]

$$I = (e/h)\int {\rm d}\epsilon T_{\rm LR}(\epsilon)[f_{\rm L}(\epsilon) - f_{\rm R}(\epsilon)],$$

where $f_{\rm L/R}(\epsilon) = 1/\{\exp[(\epsilon - \mu_{\rm L/R})/k_B T] + 1\}$ is the Dirac–Fermi distribution function of the left and right FM leads and $T_{\rm LR}(\epsilon) = \mathbf{Tr}[\mathbf{\Gamma_L G^r \Gamma_R G^a}]$ is the transmission coefficient, with the line-width function $\mathbf{\Gamma}_\alpha(\boldsymbol{\epsilon}) = {\rm i}[\mathbf{\Sigma}^{\rm r}_\alpha(\boldsymbol{\epsilon}) - \mathbf{\Sigma}^{\rm a}_\alpha(\boldsymbol{\epsilon})]$ and Green's functions $\mathbf{G^r}(\boldsymbol{\epsilon}) = [\mathbf{G^a}(\boldsymbol{\epsilon})]^\dagger = \mathbf{1}/[\boldsymbol{\epsilon} - \mathbf{H_C} - \mathbf{\Sigma^r_L} - \mathbf{\Sigma^r_R}]$. $\mathbf{\Sigma^r_{L/R}}$ is the retarded self-energy function coupling to the leads, which has to be calculated numerically by solving the surface Green function of the leads [28, 29]. After solving the current I, the linear conductance G can be obtained straightforwardly, $G = \lim_{V\to 0} {\rm d}I/{\rm d}V$, with the bias $V = \mu_{\rm L} - \mu_{\rm R}$. At zero temperature $G = (e^2/h)T(E_{\rm F})$. In the numerical calculation, we take the nearest-neighbor hopping energy $t = 1$ as the energy unit and adopt the Dirac point energies $\epsilon_{\rm L} = \epsilon_{\rm R} = \epsilon_{\rm C} = 0$. The magnetizations M_α in the left and right FM leads are assumed to be equal ($M_{\rm L} = M_{\rm R} = M$), which is usually reasonable when the two FM leads are made of the same material. The angle $\varphi = 0$ because the conductance and MR are independent of φ.

3. The case of the zigzag edge

In this section, we focus on the zigzag edge graphene-based spin valves. We first investigate the conductance G on the parallel and antiparallel configurations, and then the MR and the conductance with arbitrary angles between the magnetizations $\mathbf{M}_{\rm L}$ and $\mathbf{M}_{\rm R}$.

3.1. The conductance for the parallel configuration

Figures 1(b) and (c) show the conductance G versus the Fermi energy $E_{\rm F}$ for different magnetizations, M, of the parallel configuration (i.e. $\theta = 0$). When the magnetization $M = 0$, the two leads are normal and the whole device is a flawless graphene ribbon. In this case, the conductance G exhibits a plateau structure with plateau values at $2, 6, 10, \ldots$ (in the unit e^2/h), i.e. at the half-integer position, $g(n + 1/2)e^2/h$ with the degeneracy $g = 4$, due to the transverse subband structures. The step height of the value $4e^2/h$ results from spin and valley degeneracy and the plateaus at half-integer values originates from the fact that the zeroth subband has the only spin degeneracy.

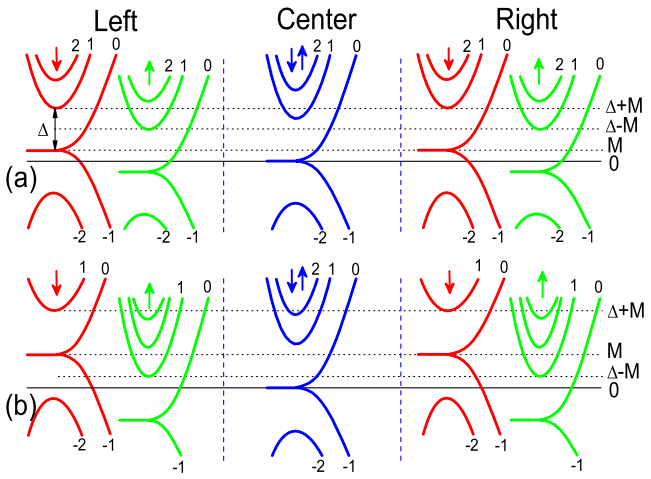

Figure 2. The energy band structures of the left lead, center region, and right lead in the case of a zigzag edge in the parallel configuration ($\theta = 0$). (a) $0 < M < \triangle/2$ and (b) $\triangle/2 < M < \triangle$.

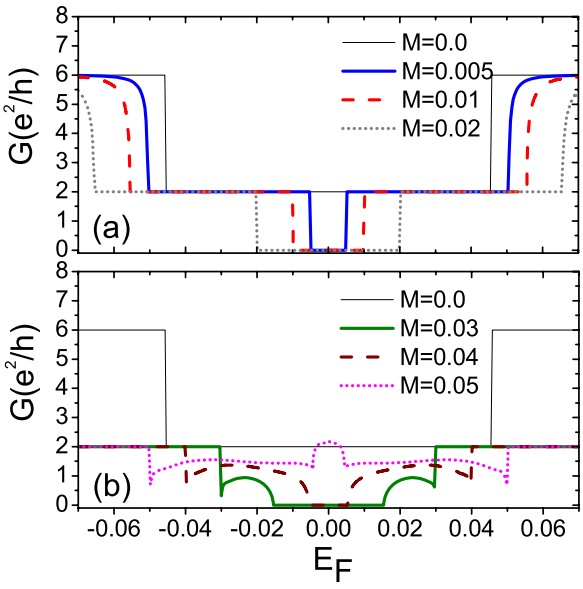

Figure 3. The conductance G versus the Fermi energy E_F for different M in the antiparallel configuration ($\theta = \pi$). The size of system is the same as figure 1(b).

When the two leads are FM with a non-zero M, the conductance G does not have the perfect plateau structure, but still obeys the electron–hole symmetry, $G(-E_F) = G(E_F)$ (see figures 1(b) and (c)). In the following, we discuss the conductance G in detail for $0 < M < \triangle/2$ and $\triangle/2 < M < \triangle$, where $\triangle$ is the energy splitting between the first subband and the zeroth subband (see figure 2) and $\triangle \approx 0.045$ for $N = 50$. For $0 < M < \triangle/2$, the curve of G versus E_F can be partitioned into several regions: $(0, M)$, $(M, \triangle - M)$, $(\triangle - M, \triangle + M)$, etc. In the first interval, $E_F \in (0, M)$, the conductance G oscillates with a value between e^2/h and $2e^2/h$. In the interval, $E_F \in (M, \triangle - M)$, the conductance G is exactly equal to $2e^2/h$ and forms a plateau. In the interval, $E_F \in (\triangle - M, \triangle + M)$, the conductance approaches the value $4e^2/h$. With a further rise in E_F, the conductance becomes larger.

In order to understand the above results, we present the energy bands of the left lead, center region, and right lead in figure 2, and the band index is specified in each region. Owing to the symmetry of bands, only part of the moment $k > 0$ is shown. The 0th and -1th subbands in the FM leads are nondegenerate, but other subbands are two-fold degenerated. Because of the parity conservation of the transverse wavefunction, the electrons belonging to the even (odd) parity subbands in the left FM lead are transported only into the even (odd) parity subbands of the right lead, which was demonstrated in a very recent letter [30] and it is termed the band-selective phenomenon. For convenience, we use the symbol (i, j, k) to denote the channel through which electrons are transported from the ith band of the left lead, through the jth band in the center region, to the kth band of the right lead, and $T_{i,j,k}$ to denote its transmission coefficient.

With the aid of the energy bands in figure 2(a), we now explain the conductance G in figure 1(b) with $0 < M < \triangle/2$. (i) When $E_F \in (0, M)$, the channel $(0, 0, 0)$ is open for spin-up electrons, and $T_{0,0,0}$ is exactly 1 due to lack of scattering. For spin-down electrons, the channel $(-1, 0, -1)$ is open, in which the parity of the transverse wavefunction in the center region mismatches with that of the left and right lead, so that scattering exists and $0 < T_{-1,0,-1} < 1$. As a result, the total conductance oscillates with a value between e^2/h and $2e^2/h$. (ii) When $E_F \in (M, \triangle - M)$, the channels $(0, 0, 0)$ are available for both the spin-up and spin-down electrons, and the conductance G exactly equals $2e^2/h$. (iii) Further, when E_F increases to the range of $(\triangle - M, \triangle + M)$, besides the channels $(0, 0, 0)$ of both spin electrons, the channels $(1, j, 1)$ $(j = 0, 1)$ of the spin-up take part in the transport, which make the conductance G approximately $4e^2/h$.

Now we discuss the conductance in the case of $\triangle/2 < M < \triangle$. Figure 1(c) shows the conductance, and the corresponding band structure is shown in figure 2(b). Apparently, the conductance G varies in a more complex way than that in $0 < M < \triangle/2$ (see figures 1(b) and (c)). Here we are mainly concerned with two energy regions: $E_F \in (0, \triangle - M)$ and $(\triangle - M, M)$. When $E_F \in (0, \triangle - M)$ the transport involves the channel $(0, 0, 0)$ of spin-up electrons and the channel $(-1, 0, -1)$ of spin-down electrons. So the conductance G oscillates between e^2/h and $2e^2/h$, which is identical with case (i) when $0 < M < \triangle/2$. For $E_F \in (\triangle - M, M)$, another channel $(1, 0, 1)$ of spin-up electrons joins into the transport, so the conductance is obviously enhanced and the value lies between $2e^2/h$ and $4e^2/h$. Further, for $E_F > M$, because more channels will be opened, the conductance usually becomes larger than $4e^2/h$.

3.2. The conductance for the antiparallel configuration

Next, we study the antiparallel configuration with $\theta = \pi$. The results for the conductance G are shown in figure 3. One of the main characteristics is a zero conductance when E_F is near the Dirac point (i.e. $E_F = 0$). This is very different from the parallel configuration, in which G is always larger than e^2/h. Let us analyze the conductance in detail in the

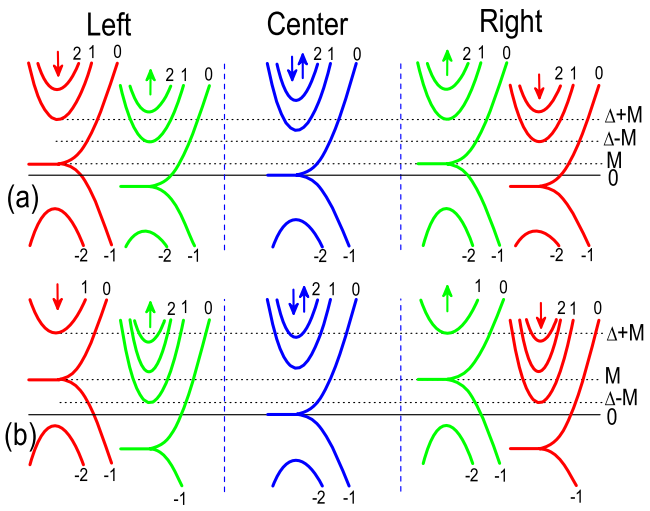

Figure 4. The energy band structures of the left lead, center region, and right lead for the zigzag edge case in the antiparallel configuration ($\theta = \pi$). (a) $0 < M < \triangle/2$ and (b) $\triangle/2 < M < \triangle$.

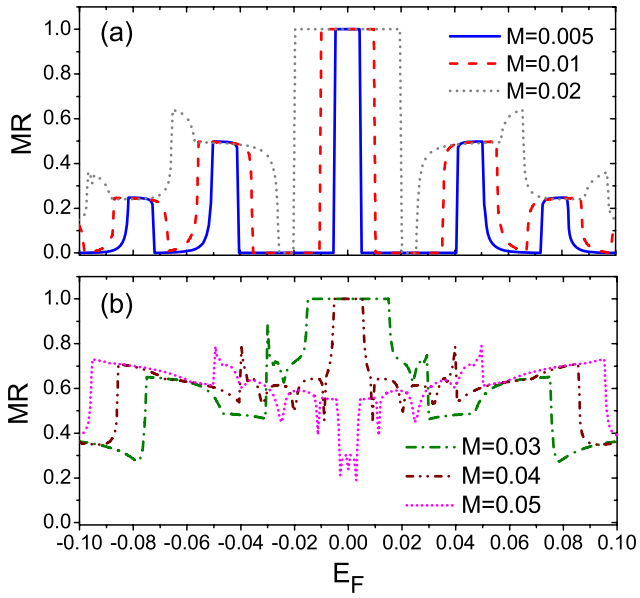

Figure 5. MR as a function of E_F for different magnetizations M. The size of the central region is $N = 50$ and $L = 10$.

following. Because $G(-E_F) = G(E_F)$, we only discuss the case $E_F > 0$. (i) For $0 < M < \triangle/2$, the conductance G is exactly zero in the range $E_F \in (0, M)$ and becomes $2e^2/h$ when $E_F \in (M, M + \triangle)$. (ii) For $\triangle/2 < M < \triangle$, $G = 0$ when $E_F \in (0, \triangle - M)$, while G is between 0 and $2e^2/h$ when $E_F \in (\triangle - M, M)$ and is exactly $2e^2/h$ when $E_F \in (M, M + \triangle)$. (iii) If M increases sequentially ($M > \triangle$), around the Dirac point a small salient appears instead of the zero conductance range.

These characteristics of conductance can be understood well from their band structures in figure 4. From the band structures of the antiparallel configuration the spin-up and spin-down electrons contribute equally to the conductance, and we only discuss the spin-up electrons in the following. (i) We discuss the case of $0 < M < \triangle/2$, and the corresponding energy band structure is illustrated in figure 4(a). When $E_F \in (0, M)$, only the channel $(0, 0, -1)$ is involved, in which the band is even parity in the left lead and is odd in the right lead. Because of the band-selective rule, its transmission coefficient $T_{0,0,-1} = 0$, and $G = 0$. On the other hand, when $E_F \in (M, \triangle + M)$, the channel $(0, 0, 0)$ is available, so that $G = 2e^2/h$. On further increasing E_F, more channels are opened and the conductance is larger. (ii) We analyze the case of $\triangle/2 < M < \triangle$, and the corresponding energy band structure is illustrated in figure 4(b). For $E_F \in (0, \triangle - M)$, only the channel $(0, 0, -1)$ is involved. So $G = 0$ because of the band-selective rule. When $E_F \in (\triangle - M, M)$, the channel $(1, 0, -1)$ is opened. The parity of the transverse wavefunction in the center region is different from those in the left and right leads. The incident electrons may be scattered and $T_{1,0,-1}$ lies between 0 and 1. As a result, $0 < G < 2e^2/h$, including the spin-down electrons. On increasing E_F to the range $(M, \triangle + M)$, the channel $(0, 0, 0)$ is opened, and the total conductance $G = 2e^2/h$. Notice that when E_F is close to, but less than, $\triangle + M$, although the extra channel $(2, 0, 0)$ is involved, the conductance G is still $2e^2/h$ because only the subband 0 is available in the right FM lead.

3.3. The magnetoresistance

After obtaining the conductances G_P and G_A of parallel and antiparallel configurations, the MR, defined as $MR = (G_P - G_A)/G_P$, can be obtained straightforwardly. Figure 5 shows the MR versus the Fermi energy E_F for different magnetizations M. Here the MR can be very large, as much as 100%, when E_F is close to the Dirac point. In particular, a plateau with the value 100% is clearly exhibited in the curve of MR-E_F. This 100% MR plateau emerges due to the zero conductance in the antiparallel configuration (see figure 3). It is noticeable that the conductance for the parallel configuration is still quite large ($>e^2/h$). This means that the present device not only has a large MR but also has a large variance of the conductance between the parallel and antiparallel configurations. Thus it is a good candidate for the spin valve devices. The width of the 100% MR plateau is determined by the magnetization M and the energy splitting $\triangle$ between the subbands. When $0 < M < \triangle/2$, its width is $2M$, so it increases with the enhancement of M. At $M = \triangle/2$, the plateau width reaches its widest value $\triangle$. On further increasing M, the plateau width becomes narrow and it is equal to $2(\triangle - M)$ when $\triangle/2 < M < \triangle$. At $M = \triangle$, the 100% MR plateau disappears. When $M > \triangle$ a valley, instead of the plateau, appears in the vicinity of $E_F = 0$. Therefore for a larger $\triangle$, it is more favorable for the formation of the 100% MR plateau. In experiment, graphene nanoribbons with widths of several-tens or sub-ten nanometers have been fabricated [24]. Taking a 20 nm wide ribbon as an example, its $\triangle$ is about 0.12 eV, which is usually much larger than M. In addition, when E_F deviates far from 0 (i.e. the region of the 100% plateau), the MR may be quite small (see figure 5). This implies that the capability of the graphene-base spin valve is optimal when it works near the Dirac point.

We study the influence of the size of the ribbon between two FM leads on the MR. Figure 6(a) (figure 6(b)) shows the

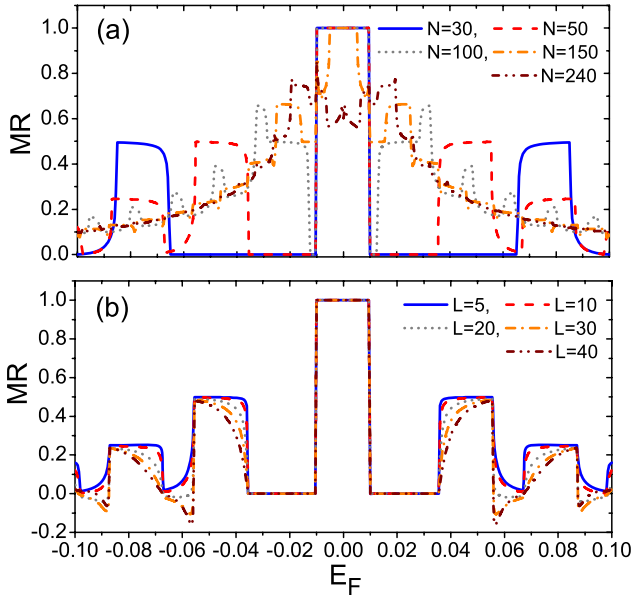

Figure 6. (a) The MR versus E_F for different widths N with length $L = 10$ and (b) MR versus E_F for different lengths L with width $N = 50$. The magnetization $M = 0.01$.

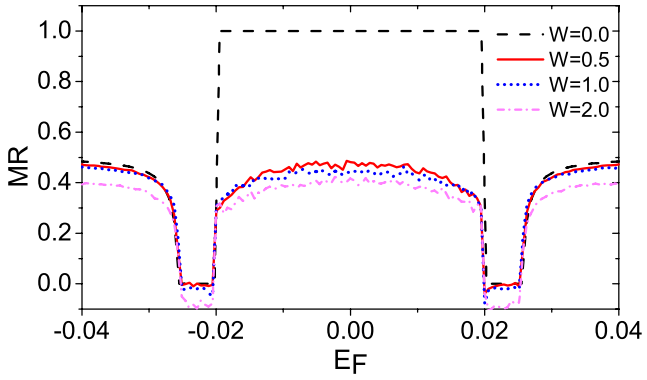

Figure 7. MR versus E_F for different disorder strength W. The parameters are $M = 0.02$, $N = 50$ and $L = 10$.

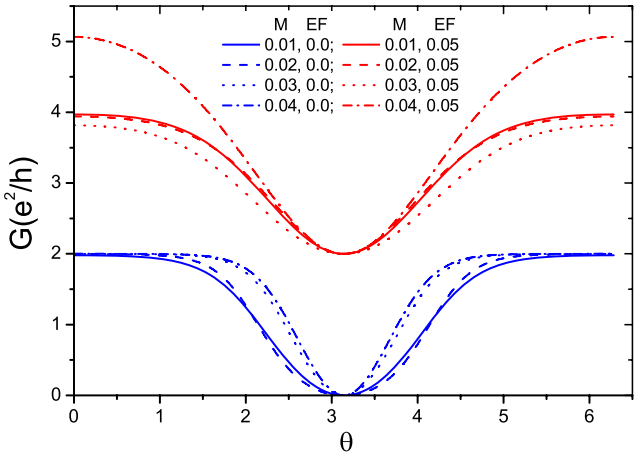

Figure 8. The conductance G versus the angle θ for different magnetization M and different Fermi energy E_F. The size of the central region is $N = 50$ and $L = 10$.

MR as a function of E_F for different widths N (lengths L) and a fixed L (N). With an increase of width N, the separation $\triangle$ of the transverse subbands decreases monotonously (with $\triangle \approx 3\pi t/4N$) [31]. Initially, the 100% MR plateau is not affected until $\triangle/2 < M$ (see the curve with $N = 30$, 50, and 100 in figure 6(a)). Then on further increasing N, the 100% MR plateau becomes narrow (see the curve with $N = 150$ in figure 6(a)), and disappears at the width N with its $\triangle = M$. Finally, when the ribbon is very wide with its $\triangle \ll M$, the MR is very small regardless of the other parameters. This result is the same as from recent work studying the infinite wide graphene spin valve device [20]. Therefore, it is favorable to select narrower nanoribbons to fabricate spin valves. On the other hand, a length change of the central region does not affect the 100% MR plateau at all (see figure 6(b)). Only the shapes of some subplateaus are slightly changed.

In the above discussion, we assumed that the Dirac point energy ϵ_C of the central region is equal to ϵ_α of the left and right leads. If ϵ_C departs from ϵ_α, the conductance G in the antiparallel configuration is still zero when $E_F \in (-M, M)$ and $0 < M < \triangle/2$, because the parity of the transverse wavefunctions in the left and right FM leads can not match each other. However, the conductance G for the parallel configuration is very large ($>e^2/h$). So the 100% MR plateau is not affected by ϵ_C slightly departing from ϵ_α.

How is the 100% MR plateau affected by the disorder? Here, we consider the Anderson disorder which exists only in the central graphene region. The on-site energy ϵ_C in the central region Hamiltonian becomes $\epsilon_C + w_i$, where w_i is uniformly distributed in the range of $[-W/2, W/2]$. Figure 7 shows the MR versus E_F at different disorder strength W, in which every MR curve for $W \neq 0$ is averaged over up to 1000 random configurations. The MR is reduced by the disorder, but the plateau shape still holds and the value is about 40%–50%, even with quite strong disorder.

3.4. The conductance for the arbitrary angle θ of the left and right magnetizations

Now we analyze θ dependence of the conductance. In figure 8, the conductance G as a function of the angle θ is plotted with a combination of M and E_F. Here the shape of the curves G-θ is approximatively a cosine function regardless of the parameters M and E_F. At $E_F = 0$ (i.e. at the center of the 100% MR plateau), the change quantity of the conductance G for the angle θ from 0 to π is about $2e^2/h$, which is quite large. About at $\theta = 2$, the derivative $dG/d\theta$ reaches an extreme value, but in the region of $0 < \theta < 1$, the derivative $dG/d\theta$ is quite small. On the other hand, when E_F deviates from the 100% MR plateau, the variation of the conductance G is also about $2e^2/h$, or even larger for some values of E_F (see the curves for $E_F = 0.05$ in figure 8), although the MR is about 50% there. However, in the region of MR = 0, the conductance G is independent of the angle θ (not shown here).

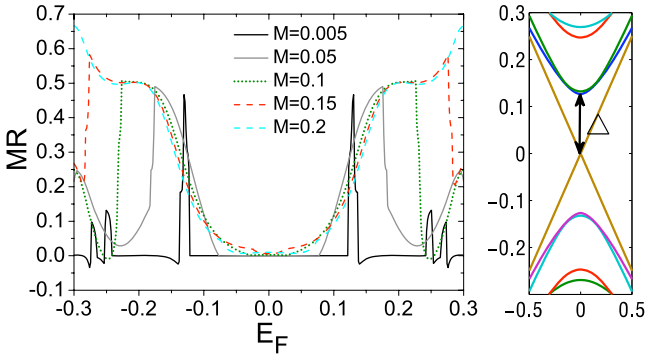

Figure 9. Left panel: MR as a function of E_F in the case of the armchair edge with the width $N = 41$ and the length $L = 40$ atomic layers in the central region. Right panel: the energy band structure of an ideal armchair edge graphene ribbon with the width $N = 41$.

4. The case of the armchair edge

In this section, we investigate the MR in the armchair edge FM/normal/FM junction. In the case of the armchair edge, there are two types of energy band structure [25]. If the number of transverse atomic layers N is equal to $3m$ or $3m + 1$ (where m is an integer), an energy gap appears. This gap can be quite large for a narrow graphene nanoribbon. When the Fermi energy E_F is in the gap, the conductance is always very small, regardless of the parallel or antiparallel configurations. So it is not interesting even if its MR is very large. For $N = 3m+2$, the graphene nanoribbon is metallic and its conductance is large.

Figure 9 shows the MR as a function of Fermi energy E_F for the metallic armchair edge FM/graphene/FM junction with $\triangle \approx 0.13t$ for $N = 41$. The conductance approaches $2e^2/h$ for both the parallel and antiparallel configurations at a large range of E_F around zero energy. As a result the MR is very small regardless of $M > \triangle$ and $M < \triangle$. On the other hand, when E_F is far away from 0 (e.g. $E_F > \triangle$), the MR can be over 50% in some regions of E_F. Anyway, the property of MR of the zigzag edge ribbon is much better than that of the armchair edge ribbon. So it is more favorable to fabricate spin valve devices by using the zigzag edge ribbon. In experiment, a graphene nanoribbon with a specific parity edge has already been successfully fabricated [24].

5. Conclusions

In summary, we have studied the electronic transport and magnetoresistance (MR) in graphene-based ferromagnetic/normal/ferromagnetic junctions where the finite width and an arbitrary relative orientation between the lead magnetizations are taken into account. For the zigzag edge case, the conductance for the parallel configuration is always larger than e^2/h under any parameter condition, but for the antiparallel configuration the conductance is exactly zero when the Fermi energy is near to the Dirac point, due to the band-selective rule. This leads to a 100% MR plateau. The 100% MR plateau is almost unaffected by the length of the central graphene region. With an increase in the width of the ribbon, the 100% MR plateau is initially kept stable, but becomes smeared in the wide ribbon limit. In the presence of disorder, the MR is slightly suppressed, but can still keep the plateau shape with the value about 50% even with quite large disorder strengths. When the orientation between the magnetizations of the two ferromagnetic leads is arbitrary, the conductance versus the relative angle θ is similar to a cosine formation. What is more, for the armchair edge case, the MR is relatively small. Therefore, it is more favorable to fabricate graphene-based spin valve devices by using zigzag edge graphene ribbons.

Acknowledgments

We gratefully acknowledge the financial support from NSF-China under Grants Nos 10525418, 10734110, and 10821403, the 973 Program Project No. 2009CB929103, and the Research Grant Council of Hong Kong under Grant No. HKU 7042/06P and HKU 10/CRF/08. Shu-guang Cheng was supported by the Science Foundation of Northwest University (No. 09NW29).

References

[1] Geim A K and Novoselov K S 2007 *Nat. Mater.* **6** 183
[2] Semenoff G W 1984 *Phys. Rev. Lett.* **53** 2449
[3] Novoselov K S, Geim A K, Morozov S V, Jiang D, Katsnelson M I, Grigorieva I V, Dubonos S V and Firsov A A 2005 *Nature* **438** 197
[4] Williams J R, DiCarlo L and Marcus C M 2007 *Science* **317** 638
[5] Novoselov K S, Geim A K, Morozov S V, Jiang D, Zhang Y, Dubonos S V, Grigorieva I V and Firsov A A 2004 *Science* **306** 666
Bolotin K I, Sikes K J, Jiang Z, Fudenberg G, Hone J, Kim P and Stormer H L 2008 *Solid State Commun.* **146** 351
[6] Tombros N, Jozsa C, Popinciue M, Jonkman H T and Van Wees B J 2007 *Nature* **448** 571
[7] Kane C L and Mele E J 2005 *Phys. Rev. Lett.* **95** 226801
[8] Yazyev O V 2008 *Nano Lett.* **8** 1011
[9] Prinz C A 1998 *Science* **282** 1660
Wolf S A, Awschalom D D, Buhrman R A, Daughton J M, von Molnár S, Roukes M L, Chtchelkanova A Y and Treger D M 2001 *Science* **294** 1488
[10] Haugen H, Huertas-Hernando D and Brataas A 2008 *Phys. Rev.* B **77** 115406
[11] Son Y-W, Cohen M L and Louie S G 2006 *Nature* **444** 347
[12] Lin H-H, Hikihara T, Jeng H-T, Huang B-L, Mou C-Y and Hu X 2009 *Phys. Rev.* B **79** 035405
[13] Hill E W, Geim A K, Novoselov K, Schedin F and Blake P 2006 *IEEE Trans. Magn.* **42** 2694
[14] Józsa C, Popinciuc M, Tombros N, Jonkman H T and van Wees B J 2009 *Phys. Rev.* B **79** 081402
[15] Han W, Wang W H, Pi K, McCreary K M, Bao W, Li Y, Miao F, Lau C N and Kawakami R K 2009 *Phys. Rev. Lett.* **102** 137205
[16] Žutić I, Fabian J and Das Sarma S 2004 *Rev. Mod. Phys.* **76** 323
[17] Saffarzadeh A and Asl M G 2009 *Eur. Phys. J.* B **67** 239
[18] Muñoz-Rojas F, Fernández-Rossier J and Palacios J J 2009 *Phys. Rev. Lett.* **102** 136810
[19] Bai C and Zhang X 2008 *Phys. Lett.* A **372** 725
[20] Brey L and Fertig H A 2007 *Phys. Rev.* B **76** 205435
[21] Ding K-H, Zhu Z-G and Berakdar J 2009 *Phys. Rev.* B **79** 045405
[22] Kim W Y and Kim K S 2008 *Nat. Nanotechnol.* **3** 408
[23] Stauber T, Castro E V, Silva N A P and Peres N M R 2008 *J. Phys.: Condens. Matter* **20** 335207

Wu Q-S, Zhang S-Z and Yang S-J 2008 *J. Phys.: Condens. Matter* **20** 485210
Zhang Z-Y 2009 *J. Phys.: Condens. Matter* **21** 095302
[24] Li X, Wang X, Zhang L, Lee S and Dai H 2008 *Science* **319** 1229
[25] Cresti A, Nemec N, Biel B, Niebler G, Triozon F, Cuniberti G and Roche S 2008 *Nano Res.* **1** 361
[26] Saito R, Dresselhaus G and Dresselhaus M S 1998 *Physical Properties of Carbon Nanotubes* (London: Imperial College Press)
[27] Datta S 1995 *Electronic Transport in Mesoscopic Systems* (Cambridge: Cambridge University Press)
[28] Lee D H and Joannopoulos J D 1981 *Phys. Rev.* B **23** 4997
[29] Sancho M P L, Sancho J M L and Rubio J 1985 *J. Phys. F: Met. Phys.* **15** 851
[30] Nakabayashi J, Yamamoto D and Kurihara S 2009 *Phys. Rev. Lett.* **102** 066803
[31] Cresti A, Grosso G and Parravicini G P 2008 *Phys. Rev.* B **77** 115408